ACS Chapter Nigeria Book of Proceedings 15th Annual Symposium
ISBN: 978-978-68-0485-9 DOI: https://doi.org/10.55455/acsnigeria.1.2.159-168

Sustainable Nanohybrid Coating from Sugarcane-Bagasse Silica and *F. sycomorus* Extract for Long-Term Corrosion Resistance of Metal Surfaces

Thompson Izuagie[1], Yusuf Salihu[2], Shehu Umar[3], and Olumuyiwa Oyekunle Akintola[1]
[1]Department of Chemistry, National Open University of Nigeria, Abuja, Nigeria
[2]Department of Pure and Industrial Chemistry Sokoto State University, Sokoto, Nigeria
[3]Department of Energy and Applied Chemistry, UsmanuDanfodiyo University, Sokoto.
***Corresponding Author's email:** tomyi2012@yahoo.com

ABSTRACT

The study reports a sustainable nanohybrid coating that integrates biogenic silica nanoparticles (SiO_2 NPs) from sugarcane bagasse with *Ficus sycomorus* leaf extract in an epoxy matrix to protect metal surfaces against corrosion. Silica was prepared by a sol–gel route from acid-leached bagasse ash and characterized usingFT-IR, XRD and SEM. The SiO_2 NPs were amorphous and silanol-rich, forming strong interfacial interactions with epoxy and creating a dense, tortuous barrier. The *F. sycomorus* extract, rich in phenolics, flavonoids, and alkaloids, served as a green inhibitor via adsorption and metal-ion complexation. Coatings containing only extract (P), only silica (NP), and the combined nanohybrid (NH) were applied to tin-plate and evaluated by neutral salt spray (up to 360 h) and NaCl immersion. Relative to neat epoxy, all modified films reduced degradation, with NH performing best: rust creep <1 mm and corroded area ≤3% at 360 h, versus ~7 mm and >50% for the control; P and NP were intermediate (creep ≤3 mm, area ≤16–18%). Immersion testing showed corrosion-rate suppression from ~1.0×10^{-4} mm·h^{-1} (control) to <2.0×10^{-5} mm·h^{-1} (NH) with inhibition efficiency >80%; NP and P achieved ~60% and ~40%, respectively. Kinetic analysis confirmed diffusion-controlled growth for all systems, with parabolic rate constants k_p decreasing from 0.0998 (control) to 0.00007 mm²·h^{-1} (NH), and power-law exponents n ≈ 0.4–0.5. The synergy between SiO_2-induced barrier densification and bio-extract chemisorption/passivation underpins the gains in durability. Leveraging agricultural waste and plant-derived inhibitors, this nanohybrid advances circular-economy coatings while delivering high corrosion resistance in saline environments.

KEYWORDS: Nanohybrid, coatings, anticorrosion, *Ficus sycomorus*, silica nanoparticles.

1. INTRODUCTION

Corrosion, the progressive deterioration of metals and alloys due to chemical or electrochemical interaction with their environment, remains a critical challenge across industries. Globally, corrosionrelated losses are estimated at 3–4% of the world's gross domestic product (GDP), underscoring its severe economic and environmental consequences for infrastructure, energy, and manufacturing sectors.[1] Beyond the economic burden, corrosion can compromise structural integrity, cause catastrophic failures, and contribute to environmental contamination.[2]Consequently, the development of durable, sustainable corrosion-protection systems has become an essential research priority.

Conventional coatings such as chromate, phosphate, and solvent-based paints provide only short-term protection and frequently suffer from poor adhesion, brittleness, and the release of volatile organic compounds (VOCs), which pose ecological and health risks.[3] In response to increasingly strict environmental regulations, efforts have intensified to design green and high-performance alternatives, including hybrid nanocomposites and plant-based corrosion inhibitors.[4] These nanocomposite and nanohybrid coatings, in which organic polymers are reinforced with inorganic nanofillers, offer improved mechanical strength, thermal stability, and impermeability due to interfacial synergy and optimized dispersion of nanoparticles.[5,6]

Among the various nanofillers, silica (SiO_2) nanoparticles stand out for their abundance, low cost, nontoxicity, and chemical stability. When incorporated into epoxy or polymer matrices, silica nanoparticles generate tortuous diffusion pathways that slow the ingress of moisture, oxygen, and chloride ions, effectively increasing corrosion resistance.[3,7] Furthermore, biogenic silica derived from agricultural residues such as sugarcane bagasse provides a renewable alternative to conventional silica sources and aligns with circular economy principles.[4] The conversion of agro-waste into functional nanomaterials not only reduces environmental burden but also adds economic value to biomass waste streams.

In parallel, bioactive plant extracts have emerged as powerful corrosion inhibitors. These natural substances, that are rich in phenolics, flavonoids, tannins, and alkaloids, can adsorb on metallic surfaces, forming stable protective films that suppress both anodic and cathodic reactions.[1] Such adsorption typically involves π-electron and lone-pair interactions that hinder electrochemical activity

and reduce charge transfer.[2] For instance, *F. sycomorus* extract contains multiple polyphenolic compounds capable of complexing with metal ions and promoting passivation, making it a potential green corrosion inhibitor. When combined with epoxy resin, which is a matrix known for its strong adhesion, flexibility, and chemical resistance, the result is a nanohybrid coating that merges physical barrier effects, chemical inhibition, and hydrophobic sealing.[6]

Recent studies show that hybrid coatings containing nanosilica and plant-derived inhibitors significantly reduce corrosion rates and delay degradation under salt-spray and immersion conditions.[5,7] However, systematic investigations of biogenic silica–plant–epoxy nanohybrids remain limited. In this context, the present work focuses on synthesizing and characterizing an eco-friendly nanohybrid coating composed of silica nanoparticles derived from sugarcane bagasse, *F. sycomorus* extract, and epoxy resin. The study aims to elucidate the synergistic corrosion inhibition mechanisms arising from the combination of inorganic nanofillers and organic bio-inhibitors, thereby contributing to the advancement of green, highperformance coatings for industrial corrosion protection.

2. MATERIALS AND METHODS

2.1 Materials and Reagents

Analytical-grade reagents were used throughout the study. Sugarcane bagasse was collected from Ramin Kura Market (Sokoto, Nigeria) as a precursor for silica nanoparticles, while *F. sycomorus* leaves were obtained from Gida Bahure Farm, Runjin Sambo area, Sokoto. The epoxy resin system (two-pack resin + hardener; PPG Industries) served as the polymeric matrix. Chemicals used included sodium hydroxide (NaOH, 99.0 %), sodium chloride (NaCl, 99.5 %), and hydrochloric acid (HCl, 36 %), all supplied by Qualikems India and JHD China. Distilled water was used for washing and solution preparation.Equipment employed comprised a muffle furnace (Narange Medical Ltd., India), vacuum oven (Gallenkamp, UK), scout analytical balance (OHAUS SPU-202, USA), and Fourier Transform Infrared Spectrometer (FTIR), X-ray diffractometer (XRD), and Scanning Electron Microscope (SEM) for characterization.

2.2 Pretreatment of Raw Materials

2.2.1 Sugarcane Bagasse

Bagasse fibres were washed with distilled water to remove dirt and sugars, air-dried for 48 h, ground, and sieved to obtain fine powder. The sample was calcined in a muffle furnace at 650 °C for 2 h to yield silica-rich ash. This temperature range efficiently removes organic residues while preserving amorphous silica structure.[8,9]

2.2.2 *F. sycomorus* Leaves

Leaves were rinsed with distilled water, shade-dried for 5 days, pulverized, and sieved (250 µm). The powder was stored in airtight containers until extraction.[10]

2.3 Extraction and Screening of *F. sycomorus* Phytochemicals

Sequential solvent extraction was performed using hexane, chloroform and methanol via Soxhlet apparatus for 6 h per extraction step. Filtrates were concentrated under vacuum at 45 °C to yield the crude extracts. Phytochemical screening followed standard colour-test procedures: Dragendorff's reagent for alkaloids; ferric-chloride for phenolics/tannins; Shinoda reagent for flavonoids; and Kedde's reagent for glycosides.[11,12]

2.4 Synthesis of Silica Nanoparticles from Sugarcane Bagasse

Silica nanoparticles (SiO_2NPs) were produced via a sol–gel process adapted from Ni'mah *et al*. (2023). A 10 g sample of the calcined ash was leached with 1 M HCl at 100 °C for 1 h, filtered and washed. The residue was then dissolved in 250 mL of 1 M NaOH at 100 °C for 1 h under stirring to produce sodium silicate. The filtrate was neutralized with 1 M HCl until gelation (pH ≈ 7). The gel was aged for 24 h, washed with distilled water, dried at 100 °C, and ground to yield fine amorphous SiO_2 nanoparticles. This green route valorizes agricultural waste and aligns with sustainable nanomaterial synthesis.[13,14]

2.5 Characterization of Silica Nanoparticles

FTIR spectra were obtainedon a Bruker Alpha spectrometer fitted with a Platinum ATR module in the 4000–400 cm^{-1} range to identify characteristic vibrations. XRD patterns were recorded using XRD, Philips X' Pert Pro with Cu Kα radiation (λ = 1.5406 Å) at 2θ = 5°–80°. While surface morphology was analyzed on SEM (Phonem Prox, Malysia) at 10–20 kV acceleration voltage.

2.6 Formulation of Nanohybrid Coating

The nanohybrid composite was formulated by blending silica nanoparticles and *F. sycomorus* extract with the epoxy resin at a mass ratio of 4:1 (NP:extract). The resin : hardener ratio was 80 : 20. The mixture was mechanically stirred for 10 min to achieve homogeneous dispersion. Coatings were applied to degreased tin-plate panels (50 × 25 × 1 mm) using a film applicator and cured at ambient temperature for 24 h. Similar epoxy/nanoparticle and plant-extract hybridizations have been reported.[15]Coating codes are: P = Epoxy + *F. sycomorus* extract; NP = Epoxy + SiO_2 nanoparticles;NH = Epoxy + SiO_2 + *F. sycomorus* nanohybrid.

2.7 Corrosion-Resistance Evaluation

2.7.1 Accelerated Salt-Spray Test and Surface Examination

Corrosion performance of the coated and X-scribed panels was evaluated according to ASTM B11723.[16] Samples were exposed to a continuous 5 wt % NaCl fog at 35 °C and 95 % relative humidity in a salt-spray chamber. At scheduled intervals (24, 48, 72, 96, 168, 240 and 360 h), panels were withdrawn, rinsed with deionized water, and air-dried for image analysis. Surface degradation was documented using a digital optical microscope (10×–200×, reflected bright-field illumination) following ASTM D1654 procedures.[17] Micrographs of the scribed regions were captured at fixed magnification and lighting to record rust propagation, blistering, and coating breakdown. Image analysis provided rust-creep length and corroded-area fraction, while time-to-first-rust and extent of film deterioration were noted visually. Prolonged resistance to rust initiation and lower rust-creep or corroded-area values were taken as indicators of superior coating protection.[17]

2.7.2 Immersion Test

Samples were immersed in 3.5 wt% NaCl solution at room temperature for 120 h. At intervals, specimens were cleaned, dried, and weighed. Corrosion rate (CR) was calculated by:

$$CR = \frac{87.6 \times W}{D \times A \times T}$$

where W = weight loss (mg), D = density (g cm^{-3}), A = area (cm^2), T = time (h).[18]The inhibition efficiency (η %) was derived as:

$$\eta = \frac{CR_0 - CR_i}{CR_0} \times 100$$

where CR_0 = corrosion rate without inhibitor and CR_i = rate with inhibitor.[5]

2.9 Kinetic modelling and mechanism

Time-dependent rust-creep data were fitted to two common kinetic models to infer the rate-controlling process. (i) Parabolic (diffusion) law: $L^2 = k_p t + C$, where the slope provides the parabolic constant k_p(mm² h⁻¹). (ii) Power-law model: $L = k\, t^n$; linear regression of $\ln L$vs $\ln t$yields the exponent $n$and prefactor k. Goodness-of-fit (R^2) and the extracted parameters (k_p, k, n)were used to compare coatings and to classify the predominant mechanism (diffusion-limited vs. mixed/other), consistent with current practice in corrosion-protective coatings.[19]

2.8 Data Analysis

All tests were performed in triplicate. Data were expressed as mean ± standard deviation, and comparisons among coatings were made using one-way ANOVA ($p < 0.05$). Figures and statistical plots were generated using OriginPro 2024.

3. RESULTS AND DISCUSSION

3.1 Phytochemical screening of *F. sycomorus* extract

Colour-test assays (Table 1) indicated the presence of alkaloids, glycosides, phenolics/tannins, flavonoids, saponins, terpenoids, and steroids in the aqueous/methanolic extracts. These classes are well known to physisorb/chemisorb on metal surfaces via π-systems and heteroatom lone pairs, forming compact inhibitor films that diminish both anodic dissolution and cathodic oxygen reduction—often with additional antioxidant effects that suppress intermediate ROS (radical) pathways.[11,12]Literature on green inhibitors supports this multi-pathway protection for plant-derived polyphenols and alkaloids.[1] **Table 1.** Phytochemical screening of *F. sycomorus*

Constituents	Alkaloids	Glycosides	Phenolics	Terpenoids	Saponins	Flavonoids	Tannnins	Steroids
Inference	+	+	+	+	+	+	+	+

3.2 Characterization of bio-derived Silica nanoparticles (SiO_2NPs)

The prepared silica nanoparticles were characterized using FTIR, XRD and SEM and the results are shown in Figure 1.

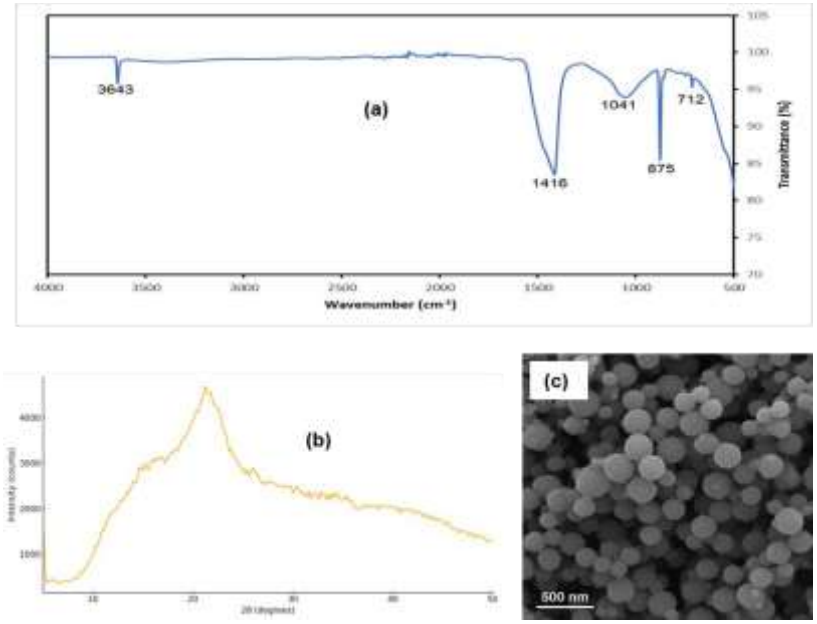

Figure 1. (a) FTIR of biogenic silica showing Si–O–Si (~1041 cm⁻¹) and Si–OH bands; (b) XRD with a broad halo at ~22° 2θ confirming amorphous SiO_2; (c) SEM revealing spherical, well-dispersed nanoparticles (~80–150 nm).

The FTIR spectrum of the synthesized silica nanoparticles (Figure 1(a))shows a prominent absorption at ~1041 cm^{-1}, which corresponds to the asymmetric stretching vibration of Si–O–Si linkages in the amorphous silica network.[20,21] Additionally, a distinct band at ~3643 cm^{-1} indicates the presence of isolated silanol (Si–OH) groups on the surface, which support the high surface reactivity and potential hydrogen-bond interactions in nanohybrid coatings.[22] Minor features at ~2326, ~1416, ~875 and ~712 cm^{-1} are attributed to adsorbed CO_2 and carbonate species, which are common in silica derived from agro-waste without extensive acid leachingand these signatures have been documented in biosilica from sugarcane bagasse and rice-husk sources.[9,23] Altogether, the FTIR data confirm formation of amorphous silica with active silanol surfaces suitable for composite coating development.

The XRD profile of the biogenic silica nanoparticles (Figure 1(b)) is dominated by a single broad diffuse halo centered near $2\theta \approx 20–22°$, with no resolvable Bragg reflections at higher angles. This is a strong signature of amorphous SiO_2 formed by short-range order of Si–O tetrahedra rather than long-range crystalline polymorphs (e.g., quartz, cristobalite). Such “amorphous hump” patterns are routinely reported for rice-husk-derived and other biosilicas and arise from medium-range correlations that produce the first-sharp diffraction peak in amorphous silica. Several studies have shown the same broad maximum at ~20–22° and used it to confirm the amorphous nature of nanosilica obtained under mild, biogenic/sol-gel conditions.[24–28] Collectively, the absence of sharp peaks and the prominence of the ~21° halo in the figure corroborate successful formation of amorphous biogenic silica with high surface area and short-range order suited for adsorption, catalysis, and biomedical functionalization.

The SEM image (Figure 1(c)) shows biogenic silica as predominantly smooth, spherical nanoparticles with limited necking or coalescence and a sub-200 nm size distribution (visually, most particles fall roughly ~80–150 nm from the 500 nm scale bar). This morphology—well-dispersed spheres produced under mild extraction/sol-gel routes—is widely reported for biosilica derived from agricultural precursors (e.g., rice husk, bamboo leaves) and is advantageous for high surface area and uniform surface silanols relevant to adsorption/catalysis and biomedical functionalization. Comparable SEM/TEM observations of spherical nanosilica are documented for rice-husk–derived mesoporous biogenic silica nanoparticles, for bamboo-leaf–derived silica synthesized via combustion–alkaline extraction, and for biosynthesized silica nanoparticles from rice husk ash, all confirming the characteristic near-monodisperse spherical morphology of amorphous SiO_2 formed via biogenic pathways.[29,30]

3.3 Corrosion performance

3.3.1 Salt-spray (fog) exposure

The salt spray test results (Figures 2 and 3) clearly demonstrate the progressive improvement in corrosion resistance achieved by the formulated coatings containing different additives (P, NP, and NH) relative to the control sample without additives.Across 360 h exposure, the control (“No additives”) shows rapid underfilm attack: rust creep reaches ~7 mm/side and corroded area approaches ~50%, evidencing fast electrolyte ingress and poor barrier integrity. Adding the plant extract alone (P) markedly slows degradation (creep $\lesssim$3 mm; area $\lesssim$16–17%), consistent with adsorption of phytochemicals (tannins/polyphenols) that complex with Fe and suppress anodic/cathodic sites – aneffect reported for *F. sycomorus* leaves acting as an efficient green inhibitor on steel and Al in acid media (reduced rates vs. blank).[10] Incorporating nano-silica alone (NP) performs comparably to P (slightly lower creep/area early on), aligning with literature where SiO_2 nanoparticles dispersed in epoxy increase tortuosity, reduce porosity, and delay chloride transport, thereby improving salt-spray durability.[31]

The NH nanohybrid (SiO_2 + *F. sycomorus*) is the clear best performer (creep <1 mm; corroded area $\lesssim$2–3% at 360 h). This synergistic improvement is consistent with hybrid epoxy–silica systems where nanoparticles provide a dense, tortuous barrier while functional organics supply active inhibition/passivation and stronger interfacial adhesion; epoxy–silica hybrid/composite coatings routinely show superior long-term salt-spray responsescompared with either component alone[32] and with modern SiO_2-based nanocontainer strategies that deliver/retain inhibitors inside epoxy to sustain protection over hundreds of hours.[33] Overall, the ranking NH $\gg$ (P $\approx$ NP) $\gg$ No-additives indicates that combining nano-silica’s barrier effect with *F. sycomorus*’s chemisorbed inhibition is additive (and likely synergistic), yielding minimal rust creep and the lowest corroded area in neutral salt spray.

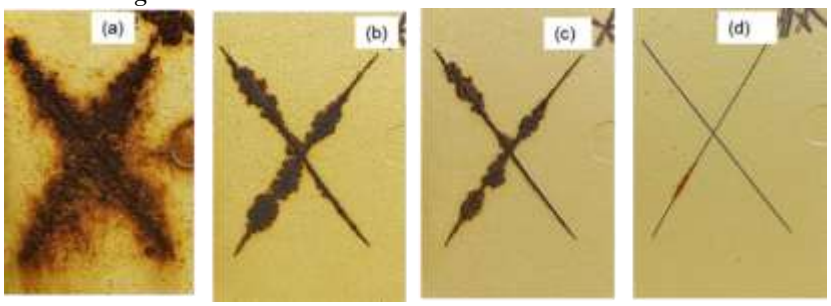

Figure 2. Visual comparison of corrosion resistance after salt spray exposure: (a) unmodified epoxy (No Additives); (b) P (epoxy + *F. sycomorus* extract); (c) NP (epoxy + SiO_2 NPs); (d) NH (epoxy + SiO_2 + *F. sycomorus* hybrid).

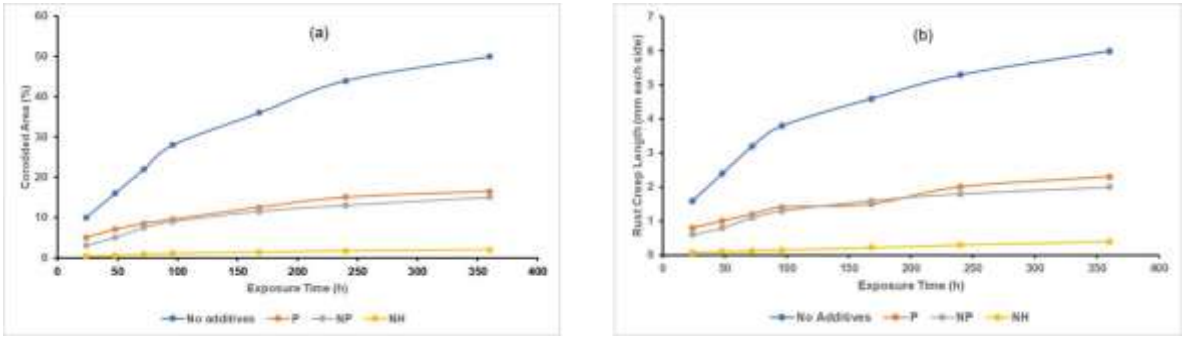

Figure 3. Salt spray test results showing (a) corroded area (%) and (b) rust creep length versus exposure time for coatings without additives, with *F. sycomorus* extract (P), SiO_2 nanoparticles (NP), and SiO_2 + *F. sycomorus* nanohybrid (NH).

3.3.2 Immersion tests (3.5% NaCl)

The immersion test data (Figure 4) reveal a clear trend consistent with the salt-spray results, confirming the synergistic corrosion protection effect of *F. Sycomorus* extract and SiO_2 nanoparticles in the epoxy matrix. The test shows a stepwise drop in corrosion rate and a matching rise in inhibition efficiency as the coating moves from unmodified epoxy to the extract-only (P), silica-only (NP), and finally the nanohybrid (NH) system. The P coating likely suppresses anodic/cathodic reactions via adsorption/complexation of polyphenolic constituents from *F. sycomorus* on the steel surface—consistent with broad evidence that plant extracts act as effective "green" corrosion inhibitors through surface adsorption and film formation on steels. The NP coating further lowers the rate by densifying the film and creating tortuous diffusion paths for water/ions; epoxy films filled with dispersed SiO_2 routinely show higher impedance and lower corrosion currents in NaCl immersion. The NH coating performs best (lowest rate, highest efficiency), reflecting complementary mechanisms: the SiO_2 nanofiller improves barrier integrity and interfacial adhesion while the bio-extract provides active inhibition at the metal/coating interface, a synergy that is well documented for epoxy–silica hybrid systems. Together, these results validate the ranking NH > NP $\gtrsim$ P > No additives for immersion resistance and align with literature on plant-extract inhibitors and silica-reinforced epoxy barriers.[32,34,35]

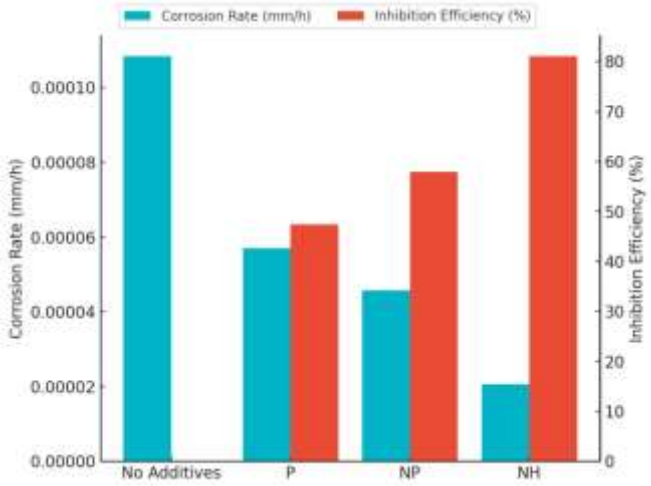

Figure 4. Corrosion rate and inhibition efficiency of epoxy coatings with and without *F. sycomorus* extract (P), SiO_2 nanoparticles (NP), and SiO_2 + *F. sycomorus* nanohybrid (NH).

3.3.3 Corrosion protection mechanism

Kinetic data (Figure 5) show that the parabolic plots (L^2 vs. time) are linear for all coatings, with strong fits (R^2 = 0.957–0.986) (Table 2), indicating diffusion-controlled rust growth through the corrosion product/coating.[19] The parabolic rate constants follow k_p: No-Additives (0.0998 mm² h^{-1}) ≫ P (0.0129) ≳ NP (0.0108) ≫ NH (7×10^{-5}). Thus, the unmodified film allows fast ionic transport through a porous rust layer, while the P film (epoxy + *F. sycomorus* extract) slows growth via an adsorbed, compact organic inhibitor film at the steel interface. NP (epoxy + SiO_2 NPs) achieves a similar k_p by densifying the matrix and imposing a tortuous diffusion path for water/Cl^-. The NH hybrid (epoxy + SiO_2 + *F. sycomorus*) suppresses rust diffusion by ~3 orders of magnitude vs. the control, consistent with synergy: nanoparticles block transport and improve cohesion/adhesion, while phytochemicals passivate active sites.[32]

Power-law fits (ln L vs. ln t) (Figure 5(b) and Table 2) give exponents n ≈ 0.52 (No-Additives), 0.39 (P), 0.45 (NP), 0.41 (NH) with high R^2 (0.978–0.991). Exponents n ≈ 0.5 are diagnostic of diffusion-limited growth, while n ≈ 0.4 reflects even stronger transport limitation by a more compact protective film. The pre-exponential factors (k) decrease in the same order, confirming the progressive reduction in effective diffusivity within the rust/coating stack. Mechanistically, these trends match classical oxidation/corrosion kinetics – parabolic scaling when transport through the product layer controls, and contemporary coating science showing that epoxy–SiO_2 hybrids markedly slow ionic ingress, whereas plant-extract inhibitors lower the interfacial reaction rate via chemisorption.[36] Overall, the kinetic hierarchy and exponents demonstrate that NH drives the system deepest into the diffusion-limited regime, yielding negligible rust creep and the smallest corroded areas.

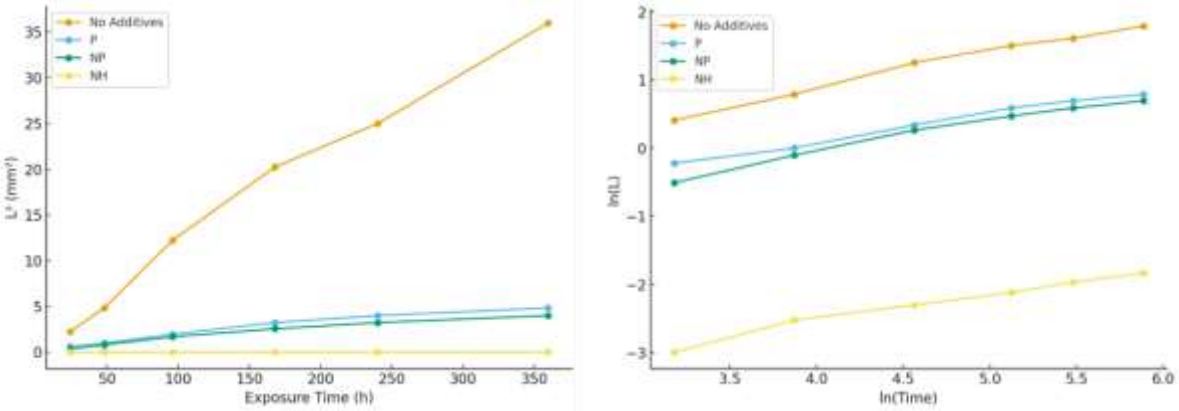

Figure 5. Kinetic analysis of rust growth for coated samples: (a) parabolic rate plots (L^2 vs. time) showing diffusion-controlled behaviour, and (b) power-law plots (ln L vs. ln t) confirming reduced corrosion rates

for coatings with *F. sycomorus* extract (P), SiO_2 nanoparticles (NP), and SiO_2 + *F. sycomorus* nanohybrid (NH).

Table 2. Kinetic fit parameters (parabolic and power-law) for rust growth of epoxy coatings with *F. sycomorus* extract and SiO_2 nanoparticles (No Additives, P, NP, NH).

Sample	Model	Rate Constant	Exponent (n)	R^2
No Additives	Parabolic	$k_p = 0.0998\ mm^2\ h^{-1}$	–	0.986
P	Parabolic	$k_p = 0.0129\ mm^2\ h^{-1}$	–	0.957
NP	Parabolic	$k_p = 0.0108\ mm^2\ h^{-1}$	–	0.957
NH	Parabolic	$k_p = 0.00007\ mm^2\ h^{-1}$	–	0.982
No Additives	Power Law	$k = e^{-1.2} \approx 0.30$	n = 0.52	0.988
P	Power Law	$k = e^{-1.5} \approx 0.23$	n = 0.39	0.991
NP	Power Law	$k = e^{-1.9} \approx 0.16$	n = 0.45	0.981
NH	Power Law	$k = e^{-4.2} \approx 0.015$	n = 0.41	0.978

4. CONCLUSION

This work shows that epoxy coatings reinforced with biogenic silica nanoparticles and *F. sycomorus* extract deliver robust, sustainable corrosion protection. The bagasse-derived silica is amorphous and silanol-rich, promoting strong interfacial bonding and a dense, tortuous barrier within the epoxy. In parallel, the plant extract supplies green inhibition via adsorption and complexation at the metal surface. When combined, these functions act cooperatively – physically blocking chloride/oxygen ingress while chemically suppressing anodic/cathodic reactions. Thus, yielding markedly lower corrosion rates, minimal rust creep, and superior stability in both salt-spray and immersion tests compared with singleadditive or neat epoxy films.Beyond performance, the nanohybrid leverages agricultural waste and bioderived chemistries, aligning with circular-economy goals and reducing dependence on synthetic inhibitors. To advance translation, future studies should apply electrochemical impedance spectroscopy for mechanism-resolved quantification, validate durability under outdoor exposure, and optimize nanoparticle and extract loadings to balance mechanical integrity with anticorrosion efficacy. Overall, *F. sycomorus*–silica–epoxy nanohybrids emerge as promising bio-inspired coatings for protecting metals in aggressive environments.

CONFLICT OF INTERESTS

The authors declare no conflict of interests.

REFERENCES

(1) Sheydaei, M. The Use of Plant Extracts as Green Corrosion Inhibitors: A Review. *Surfaces*2024, *7* (2), 380–403. https://doi.org/10.3390/surfaces7020024.

(2) Nwigwe, U. S.; Nwoye, C. I. Green Corrosion Inhibitors for Steel and Other Metals in Basic Media: A Mini-Review. *Research on Engineering Structures and Materials*2023. https://doi.org/10.17515/resm2023.643ma0116.

(3) Samad, U.; Alam, M.; Abdo, H.; Anis, A.; Al-Zahrani, S. Synergistic Effect of Nanoparticles: Enhanced Mechanical and Corrosion Protection Properties of Epoxy Coatings Incorporated with SiO2 and ZrO2. *Polymers (Basel)*2023, *15* (14), 3100. https://doi.org/10.3390/polym15143100.

(4) Hassan, I.; Baba, N. M.; Benin, M. E.; Labulo, A. H. Review on Green Synthesis of Silica Nanoparticle Functionalized Graphene Oxide Acrylic Resin for Anti-Corrosion Applications. *Journal of Umm Al-Qura University for Applied Sciences*2024, *10* (2), 379–397. https://doi.org/10.1007/s43994-023-00106-w.

(5) Ovari, T.-R.; Toth, T.; Katona, G.; Szabó, G. S.; Muresan, L. M. Epoxy Coatings Doped with (3Aminopropyl)Triethoxysilane-Modified Silica Nanoparticles for Anti-Corrosion Protection of Zinc. *Coatings*2023, *13* (11), 1844. https://doi.org/10.3390/coatings13111844.

(6) López-Campos, J. E. D.; Mojica-Gómez, J.; Maciel-Cerda, A.; Castaño, V. M.; HernándezPadrón, G. Hybrid Epoxy-SiO2/GO Nanosheets Anti-Corrosive Coating for Aeronautic Aluminum Al6061-T5. *J Coat Technol Res*2024, *21* (2), 559–574. https://doi.org/10.1007/s11998-023-00838-8.

(7) Olivieri, F.; Scherillo, F.; Castaldo, R.; Cocca, M.; Squillace, A.; Gentile, G.; Lavorgna, M. Effectiveness of Mesoporous Silica Nanoparticles Functionalized with Benzoyl Chloride in PHResponsive Anticorrosion Polymer Coatings. *ACS Appl Polym Mater*2023, *5* (8), 5917–5925. https://doi.org/10.1021/acsapm.3c00585.

(8) Ni'mah, Y. L.; Muhaiminah, Z. H.; Suprapto, S. Synthesis of Silica Nanoparticles from Sugarcane Bagasse by Sol-Gel Method. *Nano Particle*2023, *4* (1). https://doi.org/10.35702/nano.10010.

(9) Nayak, P. P.; Datta, A. K. Synthesis of SiO2-Nanoparticles from Rice Husk Ash and Its Comparison with Commercial Amorphous Silica through Material Characterization. *Silicon*2021, *13* (4), 1209–1214. https://doi.org/10.1007/s12633-020-00509-y.

(10) Ogwo, K.; Osuwa, J.; Udoinyang, I.; Nnanna, L. Corrosion Inhibition of Mild Steel and Aluminium in 1 M Hydrochloric Acid by Leaves Extracts of Ficus Sycomorus. *Physical Science International Journal*2017, *14* (3), 1–10. https://doi.org/10.9734/PSIJ/2017/32708.

(11) Ogunleye, O. O.; Arinkoola, A. O.; Eletta, O. A.; Agbede, O. O.; Osho, Y. A.; Morakinyo, A. F.; Hamed, J. O. Green Corrosion Inhibition and Adsorption Characteristics of Luffa Cylindrica Leaf Extract on Mild Steel in Hydrochloric Acid Environment. *Heliyon*2020, *6* (1), e03205. https://doi.org/10.1016/j.heliyon.2020.e03205.

(12) Bilgic, S. Plant Extracts as Corrosion Inhibitors for Aluminium and Steel in Acid Media. *DergiPark Journal,*2022, *64* (1), 20–79.

(13) Seroka, N. S.; Taziwa, R. T.; Khotseng, L. Extraction and Synthesis of Silicon Nanoparticles (SiNPs) from Sugarcane Bagasse Ash: A Mini-Review. *Applied Sciences*2022, *12* (5), 2310. https://doi.org/10.3390/app12052310.

(14) Seroka, N. S.; Taziwa, R.; Khotseng, L. Green Synthesis of Crystalline Silica from Sugarcane Bagasse Ash: Physico-Chemical Properties. *Nanomaterials (Basel)*2022, *12* (13). https://doi.org/10.3390/nano12132184.

(15) Mod, B.; Baskar, A. V.; Bahadur, R.; Tavakkoli, E.; Van Zwieten, L.; Singh, G.; Vinu, A. From Cane to Nano: Advanced Nanomaterials Derived from Sugarcane Products with Insights into Their Synthesis and Applications. *Sci Technol Adv Mater*2024, *25* (1). https://doi.org/10.1080/14686996.2024.2393568.

(16) Practice for Operating Salt Spray (Fog) Apparatus. ASTM International: West Conshohocken, PA November 1, 2019. https://doi.org/10.1520/B0117-19.

(17) Test Method for Evaluation of Painted or Coated Specimens Subjected to Corrosive Environments. ASTM International: West Conshohocken, PA September 1, 2024. https://doi.org/10.1520/D1654-24.

(18) Fontana, M. G. .*Corrosion Engineering*; Tata McGraw-Hill, 2005.

(19) Atkinson, A. Transport Processes during the Growth of Oxide Films at Elevated Temperature. *Rev Mod Phys*1985, *57* (2), 437–470. https://doi.org/10.1103/RevModPhys.57.437.

(20) Brinker, C. Jeffrey.; Scherer, G. W. .*Sol-Gel Science : The Physics and Chemistry of Sol-Gel Processing*; Elsevier Science, 2014.

(21) Socrates, George. *Infrared and Raman Characteristic Group Frequencies : Tables and Charts*; John Wiley & Sons, 2013.

(22) Zhuravlev, L. T. The Surface Chemistry of Amorphous Silica. Zhuravlev Model. *Colloids Surf APhysicochem Eng Asp*2000, *173* (1–3), 1–38. https://doi.org/10.1016/S0927-7757(00)00556-2.

(23) Azat, S.; Korobeinyk, A. V.; Moustakas, K.; Inglezakis, V. J. Sustainable Production of Pure Silica from Rice Husk Waste in Kazakhstan. *J Clean Prod*2019, *217*, 352–359. https://doi.org/10.1016/j.jclepro.2019.01.142.

(24) Khouchaf, L.; Boulahya, K.; Das, P. P.; Nicolopoulos, S.; Kis, V. K.; Lábár, J. L. Study of the Microstructure of Amorphous Silica Nanostructures Using High-Resolution Electron Microscopy, Electron Energy Loss Spectroscopy, X-Ray Powder Diffraction, and Electron Pair Distribution Function. *Materials (Basel)*2020, *13* (19). https://doi.org/10.3390/ma13194393.

(25) Biswas, P.; Dahal, D.; Elliott, S. R. Insights into the Origin of the First Sharp Diffraction Peak in Amorphous Silica from an Analysis of Chemical and Radial Ordering. *Phys Rev B*2024, *109* (10), 104207. https://doi.org/10.1103/PhysRevB.109.104207.

(26) Peralta, Y. M.; Molina, R.; Moreno, S. Chemical and Structural Properties of Silica Obtained from Rice Husk and Its Potential as a Catalytic Support. *J Environ Chem Eng*2024, *12* (2), 112370. https://doi.org/10.1016/j.jece.2024.112370.

(27) Aiello, I. W.; Höfig, T. W.; Riboulleau, A.; Teske, A. P.; Lizarralde, D.; Ash, J. L.; Bojanova, D. P.; Buatier, M. D.; Edgcomb, V. P.; Galerne, C. Y.; Gontharet, S.; Heuer, V. B.; Jiang, S.; Kars, M. A. C.; Kim, J.-H.; Koornneef, L. M. T.; Marsaglia, K. M.; Meyer, N. R.; Morono, Y.; Negrete-Aranda, R.; Neumann, F.; Pastor, L. C.; Peña-Salinas, M. E.; Pérez-Cruz, L. L.; Ran, L.; Sarao, J. A.; Schubert, F.; Khogenkumar Singh, S.; Stock, J. M.; Toffin, L.; Xie, W.; Yamanaka, T.;

Zhuang, G. Mineralization Kinetics of Biosiliceous Sediments in Hot Subseafloors. *GeochimCosmochim Acta*2024, *380*, 71–82. https://doi.org/10.1016/j.gca.2024.07.005.

(28) Falk, G.; Shinhe, G. P.; Teixeira, L. B.; Moraes, E. G.; de Oliveira, A. P. N. Synthesis of Silica Nanoparticles from Sugarcane Bagasse Ash and Nano-Silicon via Magnesiothermic Reactions. *Ceram Int*2019, *45* (17), 21618–21624. https://doi.org/10.1016/j.ceramint.2019.07.157.

(29) Pineda-Vásquez, T. G.; Casas-Botero, A. E.; Ramírez-Carmona, M. E.; Torres-Taborda, M. M.; Soares, C. H. L.; Hotza, D. Biogeneration of Silica Nanoparticles from Rice Husk Ash Using *Fusarium Oxysporum* in Two Different Growth Media. *Ind Eng Chem Res*2014, *53* (17), 6959–6965. https://doi.org/10.1021/ie404318w.

(30) Shrestha, D.; Nayaju, T.; Kandel, M. R.; Pradhananga, R. R.; Park, C. H.; Kim, C. S. Rice HuskDerived Mesoporous Biogenic Silica Nanoparticles for Gravity Chromatography. *Heliyon*2023, *9* (4), e15142. https://doi.org/10.1016/j.heliyon.2023.e15142.

(31) Alam, M. A.; Samad, U. A.; Anis, A.; Alam, M.; Ubaidullah, M.; Al-Zahrani, S. M. Effects of SiO2 and ZnO Nanoparticles on Epoxy Coatings and Its Performance Investigation Using Thermal and Nanoindentation Technique. *Polymers (Basel)*2021, *13* (9), 1490. https://doi.org/10.3390/polym13091490.

(32) Abdollahi, H.; Ershad-Langroudi, A.; Salimi, A.; Rahimi, A. Anticorrosive Coatings Prepared Using Epoxy–Silica Hybrid Nanocomposite Materials. *Ind Eng Chem Res*2014, *53* (27), 10858– 10869. https://doi.org/10.1021/ie501289g.

(33) Wang, J.; Tan, W.; Yang, H.; Rao, X.; Luo, X.; Ma, L.; Ren, C.; Mol, A.; Zhang, D. Towards Weathering and Corrosion Resistant, Self-Warning and Self-Healing Epoxy Coatings with Tannic Acid Loaded Nanocontainers. *Npj Mater Degrad*2023, *7* (1), 39. https://doi.org/10.1038/s41529-023-00360-7.

(34) Alam, M. A.; Samad, U. A.; Sherif, E.-S. M.; Poulose, A. M.; Mohammed, J. A.; Alharthi, N.; AlZahrani, S. M. Influence of SiO2 Content and Exposure Periods on the Anticorrosion Behavior of Epoxy Nanocomposite Coatings. *Coatings*2020, *10* (2), 118. https://doi.org/10.3390/coatings10020118.

(35) R. Holla, B.; Mahesh, R.; Manjunath, H. R.; Anjanapura, V. R. Plant Extracts as Green Corrosion Inhibitors for Different Kinds of Steel: A Review. *Heliyon*2024, *10* (14), e33748. https://doi.org/10.1016/j.heliyon.2024.e33748.

(36) Rani, B. E. A.; Basu, B. B. J. Green Inhibitors for Corrosion Protection of Metals and Alloys: An Overview. *International Journal of Corrosion*2012, *2012*, 1–15. https://doi.org/10.1155/2012/380217.